MEMORANDUM FOR: SAF/PAS   AUG 1 6 2002
1690 Air Force Pentagon - 5D227
Washington DC 20330-1690

FROM:

Francis G. Hinnant, Col/USAF
Associate Director of Acquisition
NPOESS Integrated Program Office
8455 Colesville Rd, Suite 1450
Silver Spring, MD 20910

SUBJECT: Paper approval for: Limb Scatter Ozone Profiling System for the NPOESS Ozone Mapping and Profiler Suite (OMPS)

Enclosed are the required ten (10) copies of the subject papers. This paper will be released at the SPIE (International Society for Optical Engineering) International Asia-Pacific Environmental Remote Sensing Symposium to be held in Hangzhou, China on October 23 - 27, 2002. It was authored and will be presented by employees of Ball Aerospace & Technologies Corporation.

The program office has reviewed the information in the attached papers and found it appropriate for public disclosure without change.

Point of contact on this matter is James W. Morris, NPOESS IPO/ADA at 301-427-2084 (Ext. 138).

Attachment: Presentation—10 copies

Limb Scatter Ozone Profiling System for the NPOESS Ozone Mapping and Profiler Suite (OMPS)

James Leitch, Ball Aerospace & Technologies Corp.

ABSTRACT

The Ozone Mapping and Profiler Suite (OMPS) for the United States National Polar-orbiting Operational Environmental Satellite System (NPOESS) consists of a two sensor suite and Level 1 and 2 data processing algorithms to produce calibrated radiance data and ozone total column and profile values. We describe the profiling system design that matches the limb-observing space sensor performance to measurement requirements of the algorithms and uses algorithm techniques to achieve the data quality needed for limb scatter-based ozone profiling.

Keywords: NPOESS, OMPS, Ozone, Limb Profile

1. INTRODUCTION

The design of the ozone profiling system for NPOESS followed an integrated sensor-algorithm development process that balances cost and risk between all elements making up the profiling system. Trade studies on sensor design used information on algorithm sensitivities and availability of augmented algorithms to judge the cost and benefit of added sensor development. An earlier paper described the sensor optical design and expected performance[1]. In this paper, we describe the system design of the limb scatter ozone profiler and provide the latest prediction of the system's expected on-orbit performance based, wherever possible, on measured component performance and test results.

The profiling technique used on OMPS is based on measurement of ozone absorption in limb-scattered solar radiation in both UV and visible wavelengths. The NPOESS requirement of at least 5 km vertical resolution led to a limb sounding instrument with the high altitude profiling (>28 km) using UV wavelengths and the lower altitude profile (tropopause to 28 km) using the visible wavelengths of the Chappuis ozone absorption band. Figure 1 shows the ozone information content of the spectra for the high altitude and low altitude cases.

Earlier studies investigating use of limb scatter as a remote sensing technique included simulations of Rayleigh scatter, and of retrievals of ozone, NO_2, and aerosol profiles[2]. Airborne multispectral (350-700 nm) limb scans were used to retrieve aerosol extinction profiles [3,4]. Space-based limb scatter measurements were made by the ultraviolet spectrometer on Solar Mesosphere Explorer (SME) and the 265 and 296 nm spectral channels were used to retrieve ozone profiles between 48 and 70 km[5]. At these altitudes multiple scattering is insignificant, thereby restricting the technique to the mesosphere and upper stratosphere. The limb scatter signature of the El Chichon volcanic cloud was observed by the visible spectrometer on SME[6]. Aruga and Heath[7] extended the theoretical basis of ozone limb scatter retrievals to longer ultraviolet wavelengths by considering multiple scattering, but this improved technique was still restricted to altitudes above ~25 km. Because of the scientific interest in the behavior of ozone at and below the ozone peak altitude, Herman et al.[8] showed that profiling could be extended down to 15 km using limb scatter measurements at 602 nm, the peak of the Chappuis

absorption band. The combined visible-ultraviolet limb scatter technique was demonstrated by the Shuttle Ozone Limb Sounding Experiment / Limb Ozone Retrieval Experiment (SOLSE/LORE) flown on STS-87 in December 1997 [9,10].

Simulated Limb Radiances
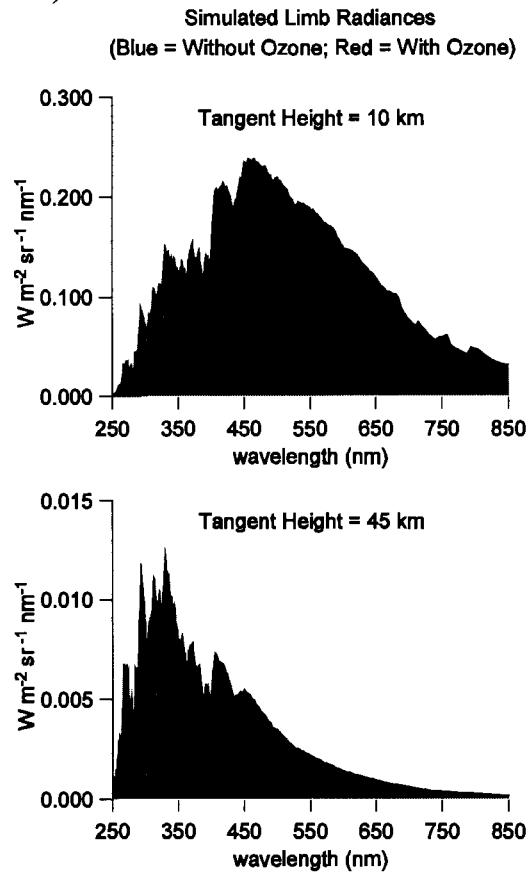**(Blue = Without Ozone; Red = With Ozone)**

Figure 1. Plots of modeled limb radiances for low altitudes (upper plot) and high altitudes (lower plot) showing the effect of absorption by ozone on the spectral content of the signals. The significantly larger absorption path of the low altitude observations show a large absorption feature in the Chappuis band centered around 600 nm.

In addition to profile retrievals, use of limb scattering for altitude registration has been investigated. The method uses near-ultraviolet limb radiances dominated by Rayleigh scatter and has been studied from a theoretical point of view[11] and using airborne data[4]. The Rayleigh scattering attitude sensor (RSAS) flown on STS-72 in January 1996 demonstrated that this technique could work from space using a limb scatter altitude profile at 355 nm[12], and it has been incorporated into SOLSE/LORE[9].

The major challenges in producing the limb scatter OMPS ozone profiling system arise from the full vertical limb radiance viewing sensor geometry and from atmospheric effects that can lead to inaccuracy and imprecision in the ozone retrieval. Sensor challenges included dynamic range coverage of the limb-scattered signal over a wide range of atmospheric conditions, careful design and fabrication of the optical and detector systems to reduce stray light, and thermal-structural stability of the sensor during changing heat loads in an orbit. The major atmospheric effects that can produce errors in the retrievals are varied surface reflectance and inhomogeneities of ozone along the sensor's line of sight. An added algorithm challenge is to derive sensor vertical pointing

information from the limb radiances in order to accurately determine the altitude scale for the retrieved profile ozone values.

2. LIMB SENSOR DESCRIPTION

The major sensor system requirements include achieving adequate signal-to-noise (SNR) ratios for the UV and visible channels, keeping stray light small enough that it does not overly degrade the accuracy of the ozone retrieval, and imaging the limb profile well enough to give 3 km vertical resolution ozone retrievals. The stability of the spectral channels between weekly solar calibrations is needed to keep accuracy errors low. All must be done within the mass allocated for the limb sensor of 12 kg (excluding cables and electronics other than CCD and its pre-amp board within the sensor).

The sensor has three telescopes, with the center telescope directed along track and the 2 side telescopes canted to ±4.25 deg crosstrack to detect limb radiances at ±250 km from the groundtrack. A cross section of the sensor illustrating the optical path is shown in Figure 2. Figure 3 shows an external view of the sensor. The vertical image sampled by each telescope covers 128 km at the limb, of which 60 km (5 to 65 km altitude) is used for the retrieval and the rest of the vertical coverage ensures that the required limb altitudes are observed even if the pointing offsets, orbital altitudes, and earth oblateness factors are at their extreme values.

Each telescope has a 10 mm and 6 mm diameter aperture to give two different brightness images on the focal plane for each view direction. The small aperture system has an additional neutral density filter that makes the total brightness ratio between images 4.5. Images are taken using long (1.7s) and short (87 ms) integration times. The combination of different brightness images and different integration times optimally divides the large dynamic range into four gain ranges.

Vertical slits are used to sample the radiance values across the entire altitude range simultaneously. The high and low gain slit images from each telescope are dispersed by a single prism and the six spectral images are formed by a two-mirror camera.

Stray light was identified as a potential major contributor to error in the ozone retrievals. The optical design used the fewest optics necessary to maintain imaging performance and low surface roughness optics are used for all elements. Low reflectivity black paint and baffles, both internal and external, are used to reduce the magnitude of any stray light in the sensor. Spectral filtering at the focal plane cuts the out-of-band stray light, the dominant stray light source for the UV and NIR spectral channels, to levels acceptable to the algorithm. Schott UV filter glass is used to achieve maximum stray light rejection for the UV channels. Figure 4 shows schematically the layout of the six spectral images and how they pass through the spectral filter before hitting the CCD. Figure 5 is a picture of the focal plane spectral filter in which alternating stripes of UV glass, visible AR, and thin film IR pass filters are laid out on the back of the focal plane assembly window.
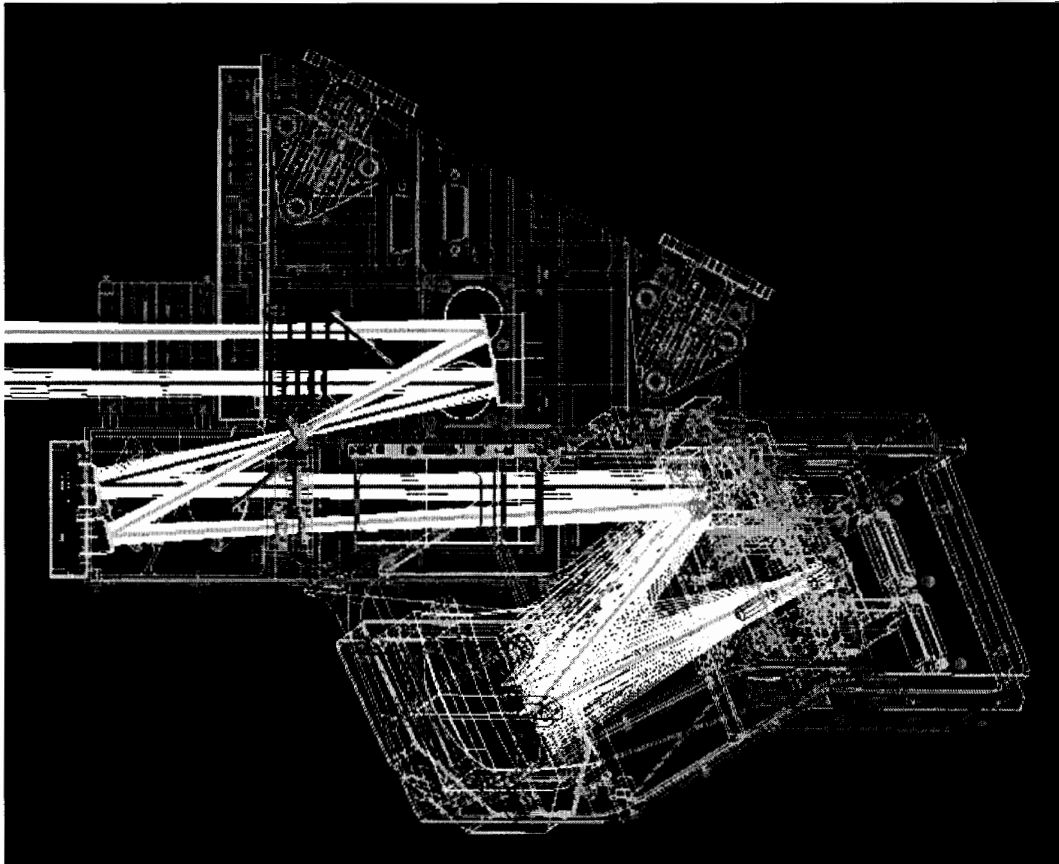
Figure 2. Cross section view of the OMPS limb sensor shows the optical path through the single mirror telescope, the slit, the collimating mirrors, the dispersing prism and the two-mirror camera system. A calibration mechanism is mounted at the telescope entrance.
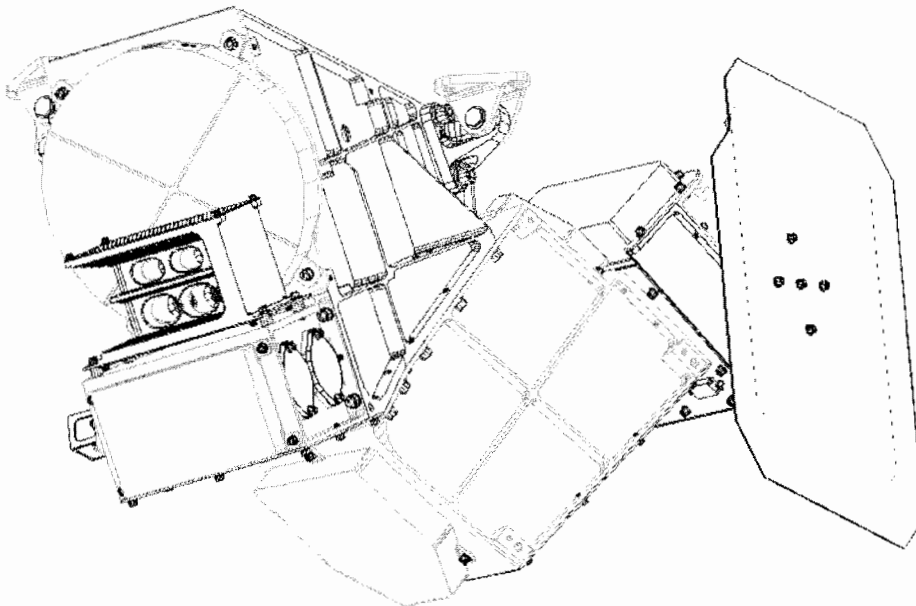

Figure 3. External view of limb sensor showing the telescope housing, camera housing, radiator for the cooled focal plane, and baffle for the entrance apertures.
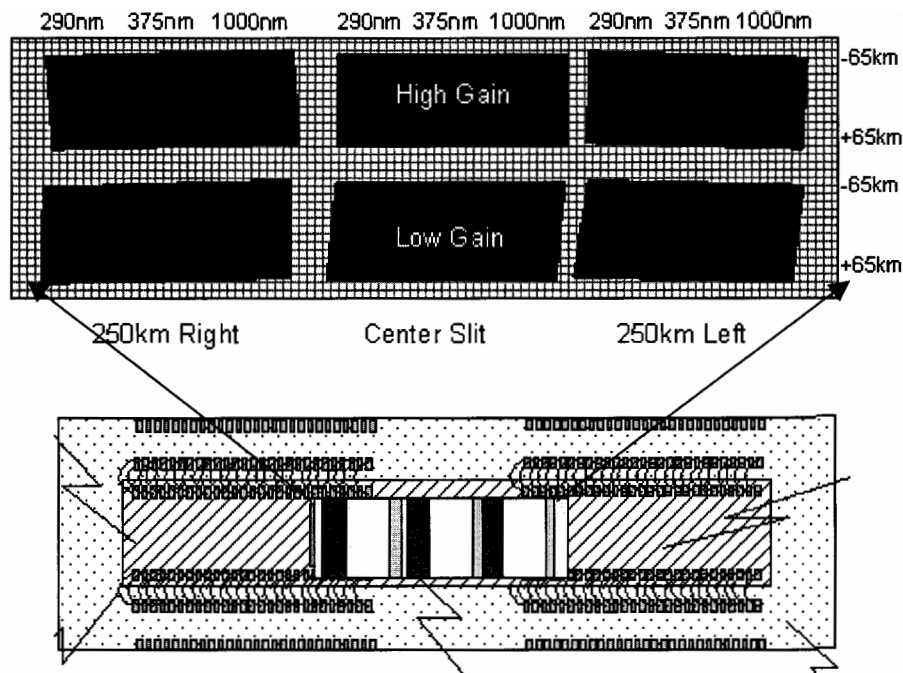
Figure 4. The six spectral images of the three vertical slits have differing widths due to the variation in dispersion between images. The spectral filters are sized so that they match the spectral image sizes and locations.
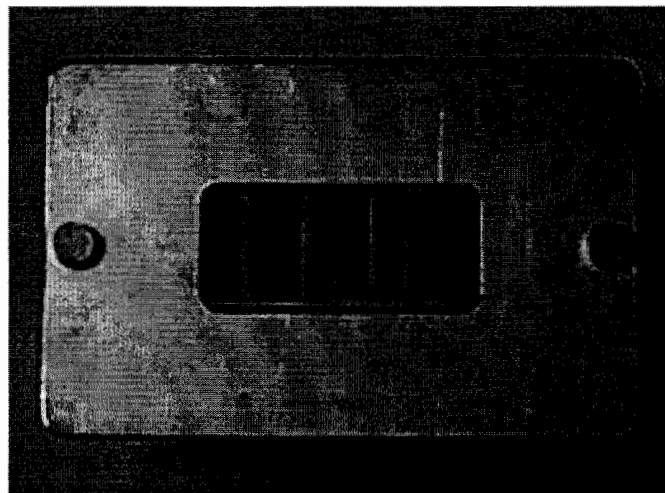

Figure 5. Picture of the 6 element filter assembly mounted on the back surface of the CCD package lid. Upon CCD package assembly, the filters end up suspended 0.2 mm above the surface of the CCD.

A full spectral image covers only 5 x 3 mm on the focal plane. The stability of the image, both in the spectral and in the spatial directions, is very important to keep ozone profile accuracy errors low. The allocated errors allow only small shifts in the spectral direction (0.01 of channel width in UV, 0.03 of width in vis/IR) and require that pointing knowledge be good to within several hundred meters at the limb. The difficulty of maintaining absolute pointing knowledge has led to adoption of scene-based altitude registration to establish sensor vertical pointing, but the spectral stability requirement remains. Thermal isolation of the sensor, both from its own baffling and from the spacecraft deck, is key to keeping thermally-induced distortions small. The isolation helps keep the optics close to uniform temperature, needed to maintain image quality, and

reduces the overall sensor's image shift sensitivity. Multi-layer insulation (MLI) is used wherever possible to keep the influence of changing thermal environment from causing spectral image shifts. Passive thermal shielding of the prism ensures that temperature-dependent refractive index effects are within acceptable limits. A map of sensor housing temperatures is shown in Figure 6. A key parameter is the thermal gradient induced in the structure. The shown case gives acceptably small thermal shifts of the spectra for the thermal conditions expected on orbit.

17.59
15.51
13.42
11.34
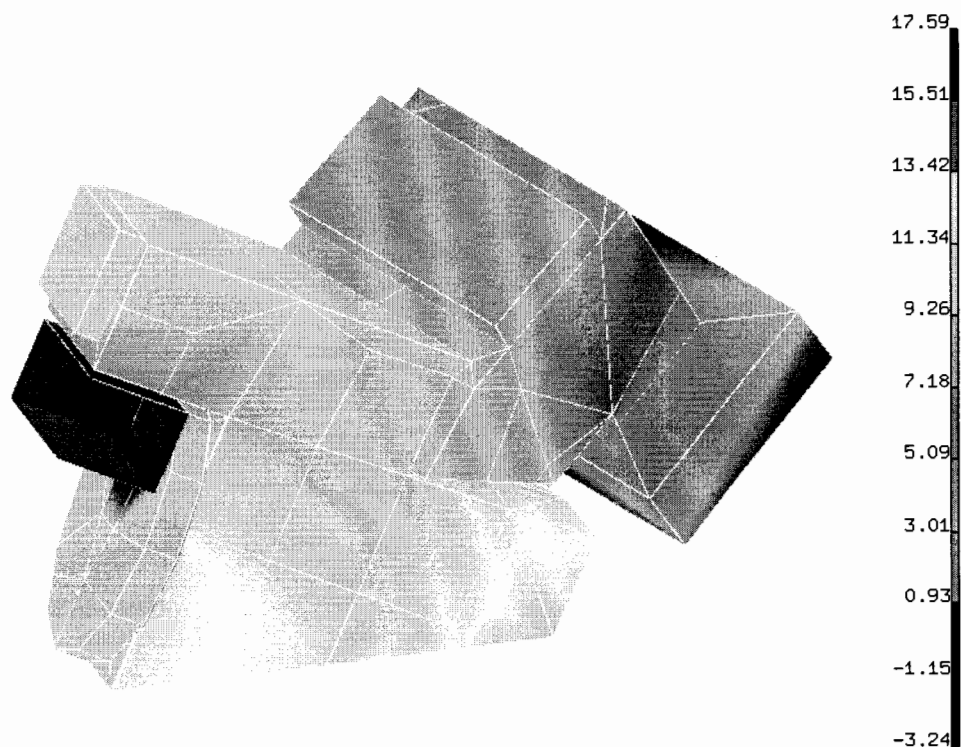9.26
7.18
5.09
3.01
0.93
-1.15
-3.24

Figure 6. Expected temperatures for a thermally-isolated, MLI-wrapped sensor shortly after eclipse exit. The cold baffle at the entrance apertures is thermally isolated from the rest of the sensor. The total gradient in temperature across the structure that supports the optical elements is ~12 degrees.

3. LIMB SENSOR PERFORMANCE

The expected performance of the sensor is predicted using estimated or measured component performance data and models to trace the component performance to overall sensor performance. The beginning-of-life values for sensor throughput are shown in Figure 7. End of life effects, including radiation darkening of the UG11 filter glass and reduced throughput due to contamination on the optics is expected to be 3 to 4% for wavelengths under 400 nm and <1% for 400 nm and above.

Given the sensor efficiency and the expected range of radiances, the UV channels up to 310 nm will all be measured with the highest gain channel (large aperture, long integration time). All other channels will be measured using multiple gain images. A key feature of the low altitude visible channels is that, for their applicable altitude range of tropopause to 28 km, the channels will be sensed in the 3 lowest gain ranges. The limitation on the SNR for these measurements is when the radiance just saturates a gain range and data must be obtained from the next lowest gain range. At this point, the relative shot noise of the measurement is at its largest, yielding the lowest SNR within the expected radiance range. This lowest SNR is boosted by taking many frames of the short integration time data (representing the two lowest gain ranges) so that coadding of the frames can boost the overall SNR. As a result, all of the visible ozone channels have similar minimum SNRs of near 2500.
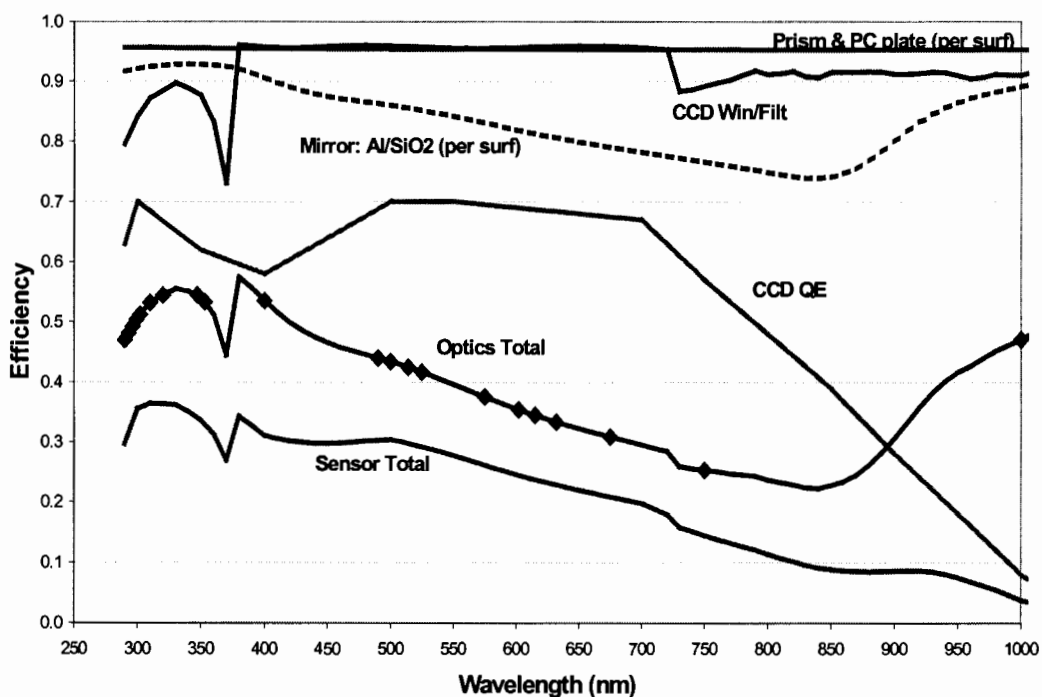

Figure 7. Expected throughput for the sensor shows the effect of the transmission band of the UG11 filter glass used for the spectral channels up to 353 nm and the loss due to other optical surfaces. The total sensor efficiency includes the CCD QE to represent a photons in to electrons out ratio.

The expected stray light at the focal plane is predicted using the surface roughness of the optics (all 8 Å rms or less) and the predicted cleanliness level of CL300. The scatter associated with these numbers is convolved with a typical radiance profile to get the expected stray light. Ghosting from the CCD window is also included. Some values of expected stray light at key wavelengths and altitudes are given in Table 1.

Altitude Range	Tropopause to 28 km		43 km to 45 km		43 km to 65 km	28 to 38 km	20 km	65 km
Wavelength Range	675 nm	750 nm	675 nm	750 nm	290 nm	320 nm	350 nm	350 nm
Stray Light	1.00%	1.20%	2.80%	7.10%	4.75%	1.10%	1.00%	1.70%

Table 1. Expected values for stray light given as a percentage of the expected signal for a given spectral channel and altitude.

Shifts of the spectral image locations during the time between weekly solar calibrations are the main effect of thermally-induced distortion that degrades the limb system performance. The dominant effect in a week is the changing thermal environment within a single orbit. Looking at the spectral channel locations on the focal plane at different points of an orbit to check if the allowed shifts are violated. Figure 8 shows that, given isolation from the spacecraft deck, the expected spectral shifts away from the nominal spectral positions as measured at the calibration point of the orbit are within allocated values.
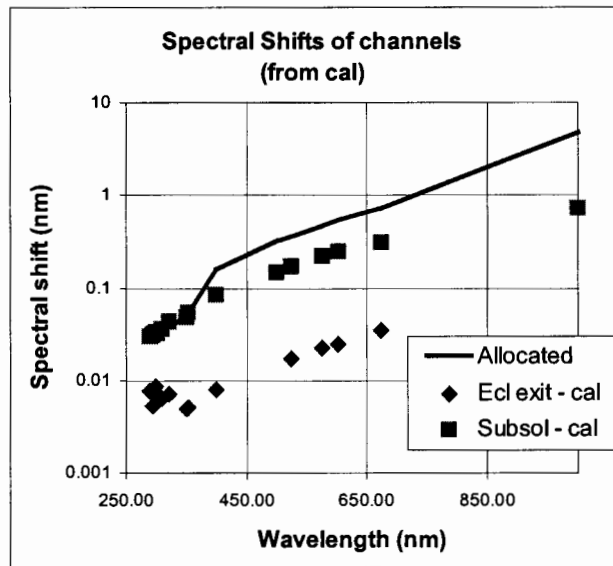

Figure 8. The figure shows the shifts in spectral channels at two points in an orbit relative to the spectral channel locations at the calibration point of the orbit. Ecl exit corresponds to the start of earth observations shortly after emerging from earth's shadow and Subsol is the point at which the spacecraft-is closest to the zenith sun condition.

4. LIMB PROFILER SYSTEM PERFORMANCE

Sensor trade studies and design have made extensive use of algorithm sensitivity studies and joint studies in which sensor performance was traced to EDR performance through simulated retrievals. The following expected performance charts offer a good summary of expected system performance given the sensor effects that have been described above. A more comprehensive description of the algorithm and its performance can be found in Ref. 13. Figure 9 shows the effect of several sensor characteristics on EDR accuracy. Figure 10 shows the expected retrieval precision, based upon the sensor SNRs. Added degradation of the retrieval precision due to scene or algorithm effects (eg, inhomogeneities of the ozone along the LOS) are being addressed by further algorithm development and use of more frequently reported radiance data than the nominal 38 s period that corresponds to a horizontal cell size of 250 km.
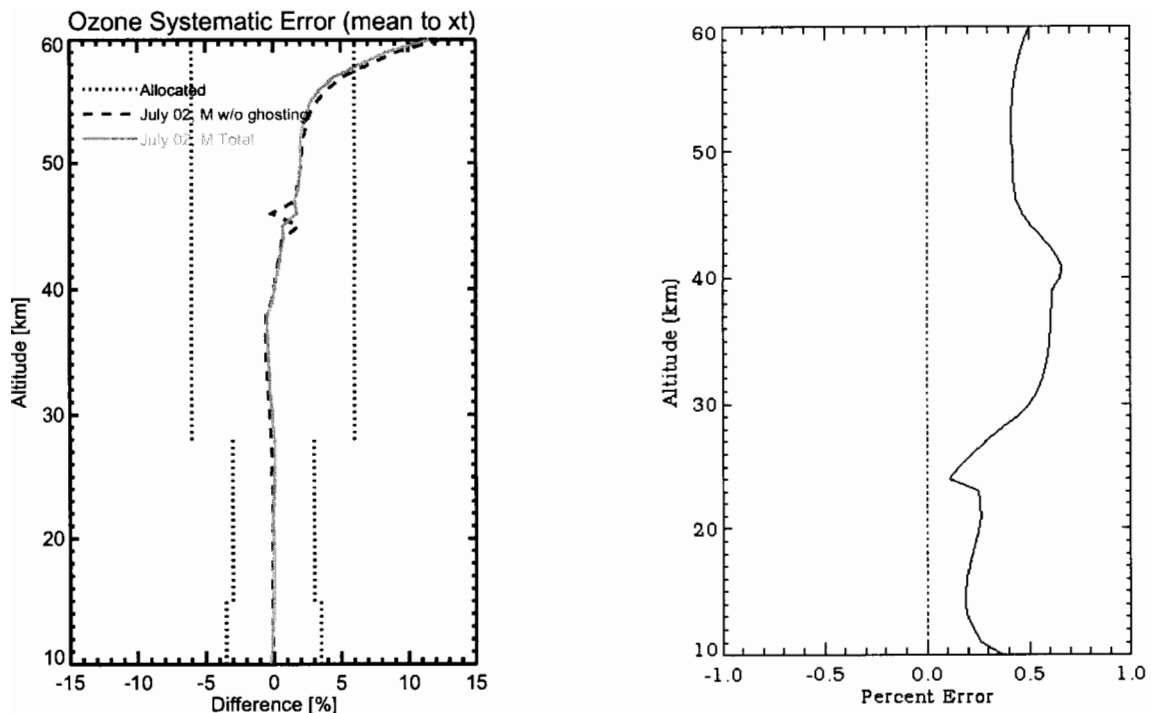
Figure 9. The left plot shows the effect of stray light on the accuracy of the ozone retrieval. Stray light performance of the limb system is within allocations for all altitudes except the top few km. The plot on the right shows the accuracy error that results from spectral shifts (and related passband changes) that are shown in Figure 8.
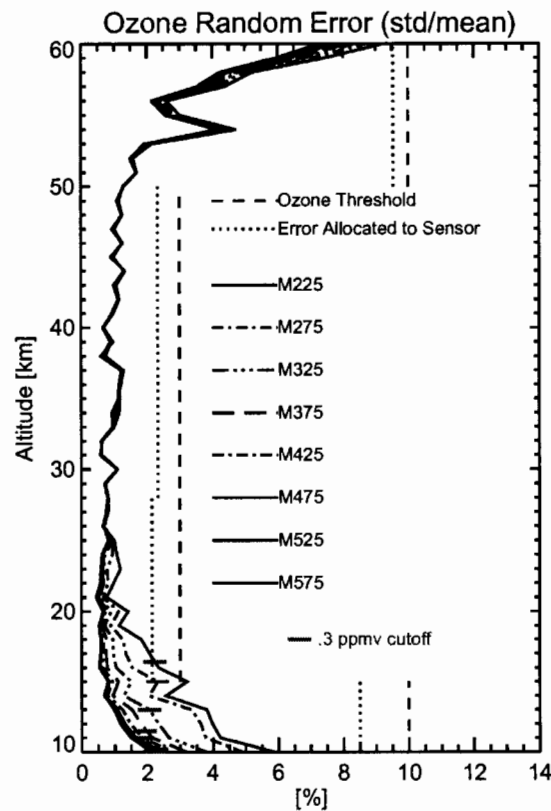

Figure 10. Expected precision of the ozone retrievals based on predicted sensor SNRs. Shown profiles are for mid-latitudes and show the 0.3 ppmv cutoff, below which the limb profiling system cannot guarantee performance.

REFERENCES

1. Dittman, Michael G., et al, Limb Broad-Band Imaging Spectrometer for the NPOESS Ozone Mapping and Profiler Suite (OMPS), *Proc. SPIE*, Seattle, Washington, 2002.

2. Malchow, H. L., and C. K. Whitney, Inversion of scattered radiance horizon profiles for gaseous concentrations and aerosol parameters, in *Inversion Methods in Atmospheric Remote Sounding*, A. Deepak, ed., pp. 215-261, Academic Press, 1977.

3. Gray, C. R., H. L. Malchow, D. C. Merritt, and R. E. Var, Aerosol monitoring by satellite horizon scanning, *J. Spacecraft Rockets, 10*, 71-76, 1973.

4. Gray, C. R., An horizon definition experiment, *AIAA Paper No. 69-869, AIAA Guidance, Control, and Flight Mechanics Conference,* 1969.

5. Rusch, D. W., G. H. Mount, C. A. Barth, R. J. Thomas, and M. T. Callan, Solar Mesosphere Explorer ultraviolet spectrometer measurements of ozone in the 1.0-0.1 mbar region, *J. Geophys. Res., 89*, 11,677-11,687, 1984.

6. Naudet, J. P., and G. E. Thomas, Aerosol optical depth and planetary albedo in the visible from the Solar Mesosphere Explorer, *J. Geophys. Res., 92*, 8373-8381, 1987.

7. Aruga, T., and D. F. Heath, Determination of vertical ozone distributions by spacecraft measurements using a limb-scan technique, Appl. Opt., 21, 3047-3054, 1980.

8. Herman, B. M., D. E. Flittner, R. D. McPeters, and P. K. Bhartia, Monitoring atmospheric ozone from space limb scatter measurements, *Proc. SPIE, 2582*, 88-99, 1995.

9. McPeters, R. D., S. J. Janz, E. Hilsenrath, T. L. Brown, D. E. Flittner, and D. F. Heath, The retrieval of ozone profiles from limb scatter measurements: results from the Shuttle Ozone Limb Sounding Experiment, *Geophys. Res. Lett., 27*, 2597-2600, 2000.

10. Flittner, D. E., B. M. Herman, and P. K. Bhartia, Ozone profiles retrieved from limb scatter measurements: theory, *Geophys. Res. Lett., 27*, 2601-2604, 2000.

11. Wolff, M., Precision limb profiles for navigation and research, *J. Spacecraft Rockets, 4*, 978-983, 1967.

12. Janz, S. J., E. Hilsenrath, D. Flittner, and D. Heath, Rayleigh scattering attitude sensor, *Proc. SPIE, 2831*, 146-153, 1996.

13. Larsen, J. IGARSS paper on limb algorithm.